Microscopic calculation of in-medium proton-proton cross sections

G. Q. Li and R. Machleidt

Department of Physics, University of Idaho, Moscow, ID 83843, U.S.A.

(February 9, 2008)

Abstract

We derive in-medium *proton-proton* cross sections in a microscopic model based upon the Bonn nucleon-nucleon potential and the Dirac-Brueckner approach for nuclear matter. We demonstrate the difference between proton-proton and neutron-proton cross sections and point out the need to distinguish carefully between the two cases. We also find substantial differences between our in-medium cross sections and phenomenological parametrizations that are commonly used in heavy-ion reactions.

The density and/or temperature dependence of hadronic systems is an interesting topic in nuclear physics. Experimentally, nucleus-nucleus collisions at intermediate energies provide a unique opportunity to form a piece of hot nuclear matter in the laboratory with a density up to 2-3ρ_0 (with ρ_0, in the range of 0.15 to 0.19 fm^{-3}, the saturation density of normal nuclear matter; in this paper we use ρ_0=0.18 fm^{-3}) [1,2]. It is thus possible to study the properties of hadrons in hot and dense media. Since this piece of dense nuclear matter exists only for a very short time (typically 10^{-23} -10^{-22} s), it is necessary to use transport models to simulate the entire collision process and to deduce the properties of the intermediate stage from the known initial conditions and the final-state observables. At intermediate energies, both the mean field and the two-body collisions play an equally important role in the dynamical evolution of the colliding system; they have to be taken into account in the transport models on an equal footing, together with a proper treatment of the Pauli blocking for the in-medium two-body collisions. The Boltzmann-Uehling-Uhlenbeck (BUU) equation [3,4] and quantum molecular dynamics (QMD) [5,6], as well as their relativistic extensions (RBUU and RQMD), are promising transport models for the description of intermediate-energy heavy-ion reactions.

Starting from the bare nucleon-nucleon (NN) interaction, in-medium NN cross sections have been calculated using relativistic [7,8] as well as nonrelativistic [9,10] Brueckner theory. In Ref. [8], we derived microscopically the in-medium *neutron-proton* (*np*) cross sections. Our derivation was based on the Bonn meson-exchange model for the NN interaction [11,12] and the Dirac-Brueckner approach [12–14] for nuclear matter. We found that our microscopic in-medium *np* cross sections deviate substantially from the phenomenological parametrization by Cugnon *et al.* [3,15] which is often used in transport model calculations.

In this Brief Report, we present now our microscopic results for in-medium *proton-proton* (*pp*) cross sections. We note that the Cugnon parametrization of NN cross sections is, in fact, a fit of the free-space *pp* data; i. e., no difference is made between *np* and *pp* scattering. However, since there are well-known differences between *pp* and *np* scattering, one should carefully distinguish between *pp* and *np* cross sections.

Proton-proton scattering occurs only in states of total isospin T=1, while np exists for T=0 and 1. This fact is responsible for the characteristic differences in the shapes of pp and np differential cross sections. This is the most crucial difference between pp and np and should by no means be ignored. Furthermore, there is the Coulomb force which is involved in pp but not in np. Finally, in the $^1S_0$ state, the strength of the strong interaction shows a small difference between pp and np which is known as charge-independence breaking (CIB). However, this is a very small effect and totally negligible in our present considerations: the in-medium effects are by an order of magnitude larger than CIB.

In general, in transport models such as BUU and QMD, the electromagnetic effects between nucleons, mainly the Coulomb interaction, are treated separately. So, what is needed are the in-medium pp cross sections due to the strong force only. Therefore, we calculate in this paper the pp cross sections without the Coulomb force. Then, the main difference between pp and np cross sections is due to the fact that in the former case only the T=1 NN channels are included while in the latter case all T=0 and T=1 states are taken into account. We note that our pp cross sections can also be used as neutron-neutron (nn) cross sections, since we neglect electromagnetic effects anyhow and the small charge-symmentry breaking, i. e., the small difference between the pp and nn strong force is totally negligible here (cf. our remark, above, concerning CIB).

In this paper, we apply exactly the the same methods as in our earlier (and more detailed) paper [8] about np cross sections to which we refer the interested reader for details. It is therefore sufficient to just sketch our method briefly here. We start from the relativistic one-boson-exchange (OBE) Bonn potential [12] which describes the two-nucleon system below 300 MeV accurately. This potential is used in (relativistic) Dirac-Brueckner calculation for nuclear matter, in which also the effective nucleon scalar and vector fields (the mean field) are determined. With this nucleon mean field and the Lorentz-boosted Pauli projector, we solve the in-medium Thompson equation (relativistic Bethe-Goldstone equation) to determine the $\tilde{G}$-matrix, from which the in-medium NN cross sections are calculted by identifying the $\tilde{G}$-matrix with the in-medium K-matrix. As in Ref. [8], we present our results in terms

the kinetic energy of the incident nucleon in the "laboratory system" (E_{lab}) in which the second nucleon is at rest. All results shown in this paper are obtained by using the Bonn A potential [12] for the bare nuclear force; in Ref. [8] we have shown that the dependence of our results on the particular model for the nuclear force is very small (as long as the model is quantitative and relativistic).

In Fig. 1, we show the differential cross section at E_{lab}=50 (a) and 200 MeV (b) for three different densities [$\rho = 0$ (solid curves), $\rho = \rho_0$ (dashed curves) and $\rho = 2\rho_0$ (dotted curves)]. At 50 MeV, the in-medium differential cross section decreases with increasing density. At 250 MeV, it decreases when going from $\rho = 0$ to $\rho = \rho_0$ and then increases. We observed a similar behavior in *np* [8]. The reason for this is that with increasing energy, the higher partial waves become more important which are less influenced by medium effects. As in the case of the *np* differential cross sections [8], we have prepared a data file, containing the *pp* differential cross sections as a function of angle, for a number of energies and densities. From this data file, the *pp* differential cross sections for any density between 0 and $3\rho_0$ and any energy between 0 and 300 MeV can be obtained with sufficient accuracy by interpolation. This data file is available from the authors upon request.

In Fig. 2, we compare the *pp* differential cross section with the *np* one at E_{lab}=100 MeV and ρ=ρ_0. Clearly there are differences between *pp* and *np*. The *pp* differential cross section is almost isotropic and has the symmetry of $d\sigma/d\Omega(\theta) = d\sigma/d\Omega(\pi - \theta)$, while the *np* differential cross section is highly anisotropic and has a profound peak at backward angles. This difference is mainly due to the fact that the T=0 states do not contribute to *pp*. In summary, Fig. 2 demonstrates clearly that one should distinguish carefully between *pp* and *np* cross sections.

In Fig. 3, we shown the *pp total* cross sections as a function of the incident energy, at ρ=0 (solid curves), $(1/2)\rho_0$ (dashed curves) and $(3/2)\rho_0$ (dotted curves). The symbols represent the exact results of our microscopic calculation, while the curves are fits in terms of a simple and practical parametrization of our results:

$$\sigma_{pp}(E_{lab},\rho) = (23.5 + 0.0256(18.2 - E_{lab}^{0.5})^{4.0})\frac{1.0 + 0.1667E_{lab}^{1.05}\rho^3}{1.0 + 9.704\rho^{1.2}} \quad (1)$$

where E_{lab} and ρ are in the units of MeV and fm^{-3}, respectively. Generaly speaking, the in-medium *pp* total cross sections decrease with increasing density and energy. For completeness, we list in Table 1 the in-medium *pp* total cross sections as function of energy and density for some selected values.

Finally in Fig. 4, we compare the *pp* total cross section with the *np* one at $\rho = \rho_0$ (a) and $(3/2)\rho_0$ (b). Also shown is the description by the Cugnon parametrization [15]. Notice that at ρ=0 (Fig. 4a), our results for the *pp* total cross section is very close to the one by Cugnon *et al.* This makes sense since the Cugnon parametrization is a fit of the Coulomb subtracted free-space *pp* scattering data. At this point, we note that, since the in-medium *pp* cross section is always smaller than the free one (see Fig. 3), the Cugnon parametrization overestimates the in-medium NN cross sections. Fig. 4a clearly demonstrates the difference between *pp* and *np* total cross sections. The *np* cross sections are much larger than the *pp* ones, especially at low energies and densities. At finite densities, this difference is reduced, since the $^3S_1$ amplitude, which contributes only in *np*, is considerable quenched in the medium. From Fig. 4 we learn again the it is important to distinguish between *np* and *pp* cross sections.

In summary, we have presented in this Brief Report predictions for in-medium *pp* cross sections derived in a microcopic way. The important conclusions are:

1. There is strong density dependence in the in-medium cross sections. Cross sections decrease in the medium. This indicates that a proper treatment of the density-dependence of the in-medium NN cross sections is important.

2. Our microscopic predictions for free-space *pp* cross sections are close to the parametrization developed by Cugnon *et al* [3,15]. However, at finite densities which are important in transport models, the Cugnon parametrization, which is density independent, overestimates the cross sections.

3. There are substantial differences between pp and np cross sections (total as well as differential). This implies that one should carefully distinguish between pp and np scattering when applying NN cross sections in transport model calculations.

Acknowledgement: This work was supported in part by the U.S. National Science Foundation under Grant No. PHY-9211607, and by the Idaho State Board of Education. One of the authors (GQL) gratefully acknowledges enlightening discussions with Prof. C. M. Ko.

REFERENCES

[1] R. Stock, Phys. Rep. **135** (1986) 259

[2] H. Stöcker and W. Greiner, Phys. Rep. **137** (1986) 278

[3] G. F. Bertsch and S. Das Gupta, Phys. Rep. **160**, 189 (1988)

[4] W. Cassing, W. Metag, U. Mosel, K. Niita, Phys. Rep. **188**, 363 (1990)

[5] J. Aichelin and H. Stöcker, Phys. Lett. **176B**, 14 (1986)

[6] J. Aichelin, Phys. Rep. **202**, 235 (1991)

[7] B. ter Haar and R. Malfliet, Phys. Rev. C **36**, 1611 (1987)

[8] G. Q. Li and R. Machleidt, Phys. Rev. C, submitted

[9] A. Bohnet, N. Ohtsuka, J. Aichelin, R. Linden and A. Faessler, Nucl. Phys. **A494**, 349 (1989)

[10] J. Jänicke, J. Aichelin, N. Ohtsuka, R. Linden and A. Faessler, Nucl. Phys. **A536**, 201 (1992)

[11] R. Machleidt, K. Holinde and Ch. Elster, Phys. Rep. **149**, 1 (1987)

[12] R. Machleidt, Adv. Nucl. Phys. **19**, 189 (1989)

[13] R. Brockmann and R. Machleidt, C **42**, 1965 (1990)

[14] G. Q. Li, R. Machleidt and R. Brockmann, Phys. Rev. C **45**, 2782 (1992).

[15] J. Cugnon, T. Mitutani and J. Vandermeulen, Nucl. Phys. **A352**, 505 (1981)

Table 1

Microscopic in-medium pp total cross sections in units of mb as derived in the present work ($\rho_0 \equiv 0.18$ fm^{-3}).

	E_{lab} (MeV)					
ρ	50	100	150	200	250	300
0	63.38	35.36	27.18	23.62	21.76	21.72
$(1/2)\rho_0$	40.03	22.84	16.75	15.59	16.29	17.28
ρ_0	26.37	17.36	14.73	14.80	15.33	16.00
$(3/2)\rho_0$	22.24	17.06	16.19	16.52	17.37	17.61
$2\rho_0$	18.50	18.60	21.06	20.61	20.35	20.10

FIGURES

FIG. 1. In-medium *pp* differential cross sections at (a) 50 MeV and (b) 200 MeV laboratory energy. Three densities are considered: $\rho = 0$ (solid line), $\rho = \rho_0$ (dashed line), and $\rho = 2\rho_0$ (dotted line). ($\rho_0 \equiv 0.18$ fm^{-3})

FIG. 2. In-medium *pp* and *np* differential cross sections at 100 MeV laboratory energy for the density $\rho = \rho_0 = 0.18$ fm^{-3}.

FIG. 3. In-medium *pp* total cross sections as function of incident energy for three densities. The symbols represent the results of our exact calculations while the curves are fits of our results in terms of the *ansatz* Eq. (1).

FIG. 4. The in-medium *pp* and *np* total cross sections at (a) ρ=0 and (b) $\rho = (3/2)\rho_0$ as obtained in our microscopic derivation (solid and dashed line, resp.) are compared to the description of NN cross sections by the Cugnon parametrization.

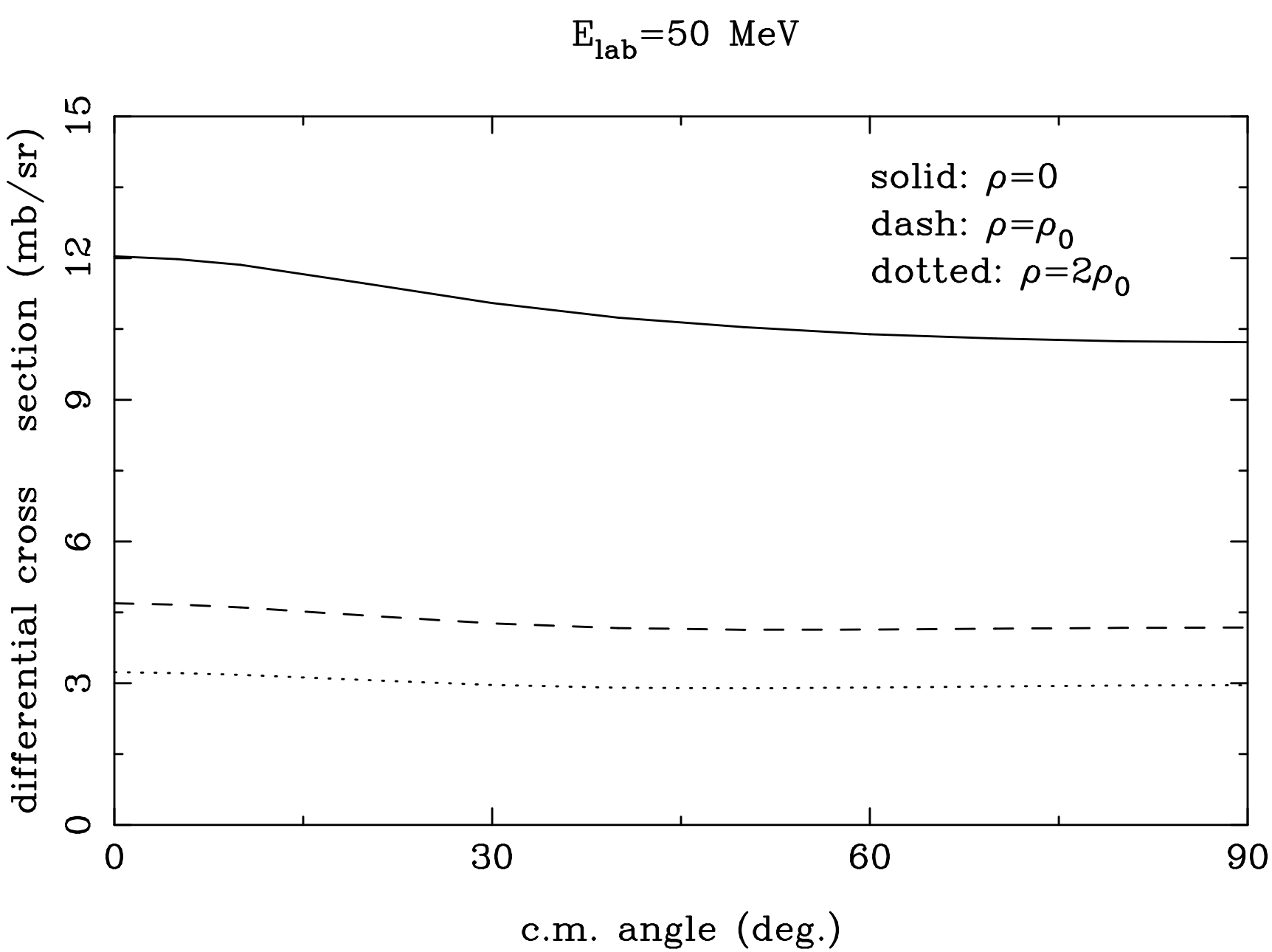
E_{lab}=50 MeV
solid: ρ=0
dash: $\rho=\rho_0$
dotted: $\rho=2\rho_0$
differential cross section (mb/sr)
0
3
6
9
12
15
0
30
60
90
c.m. angle (deg.)

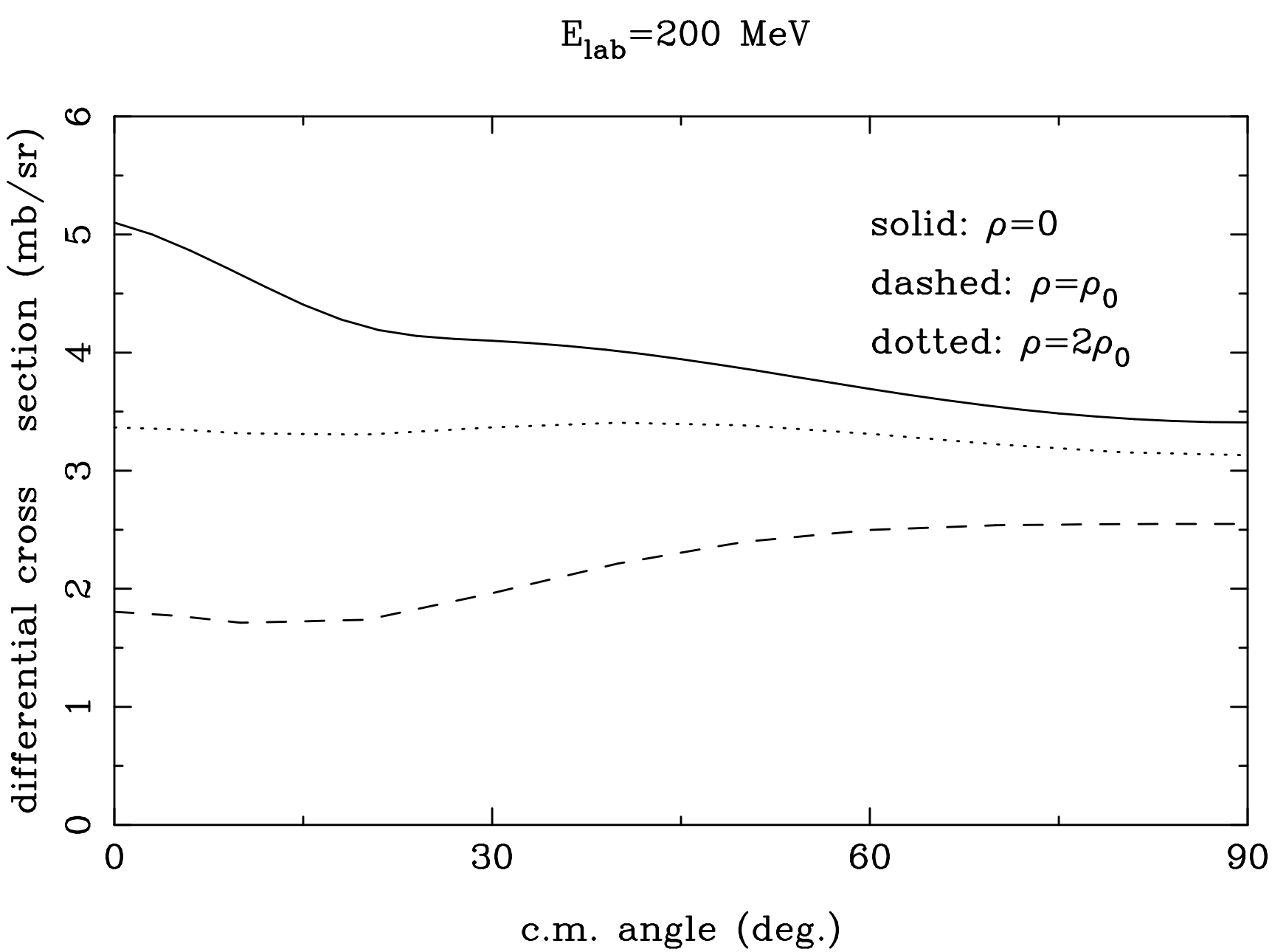
E_{lab}=200 MeV
differential cross section (mb/sr)
0
1
2
3
4
5
6
0
30
60
90
c.m. angle (deg.)
solid: ρ=0
dashed: $\rho=\rho_0$
dotted: $\rho=2\rho_0$

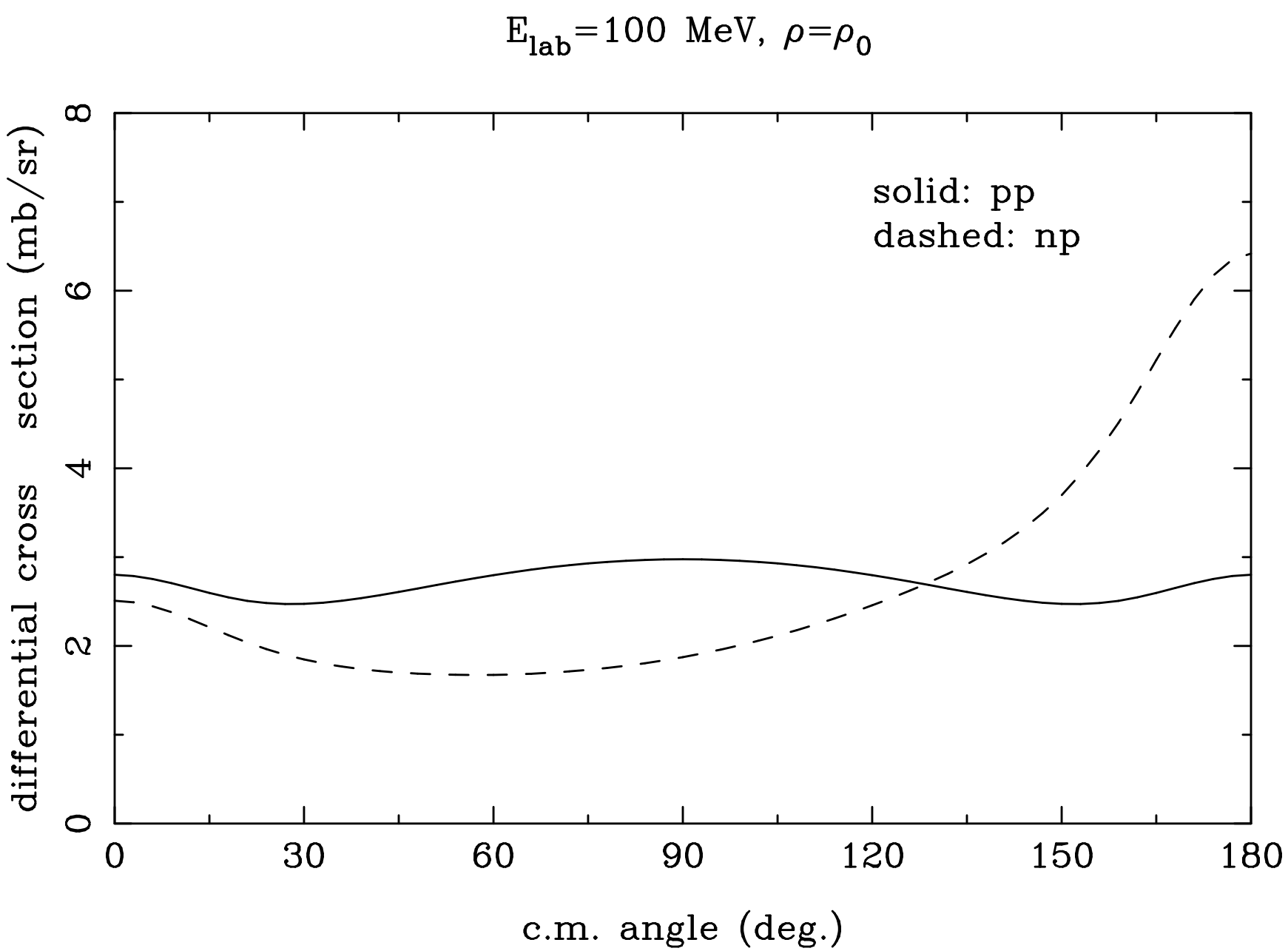
E_{lab}=100 MeV, $\rho=\rho_0$
solid: pp
dashed: np
differential cross section (mb/sr)
0
2
4
6
8
0
30
60
90
120
150
180
c.m. angle (deg.)

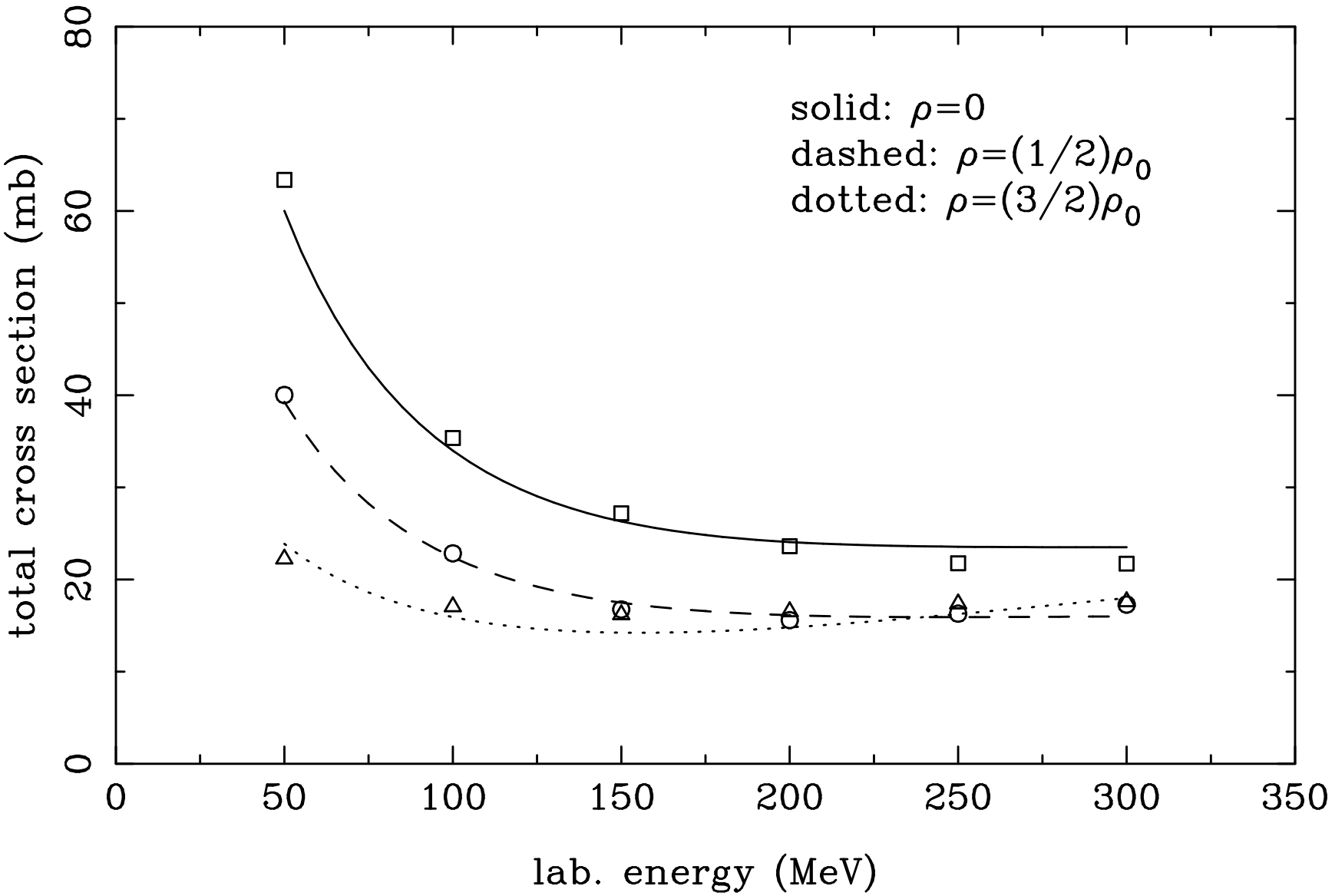
solid: $\rho=0$
dashed: $\rho=(1/2)\rho_0$
dotted: $\rho=(3/2)\rho_0$
total cross section (mb)
lab. energy (MeV)
0
20
40
60
80
0
50
100
150
200
250
300
350

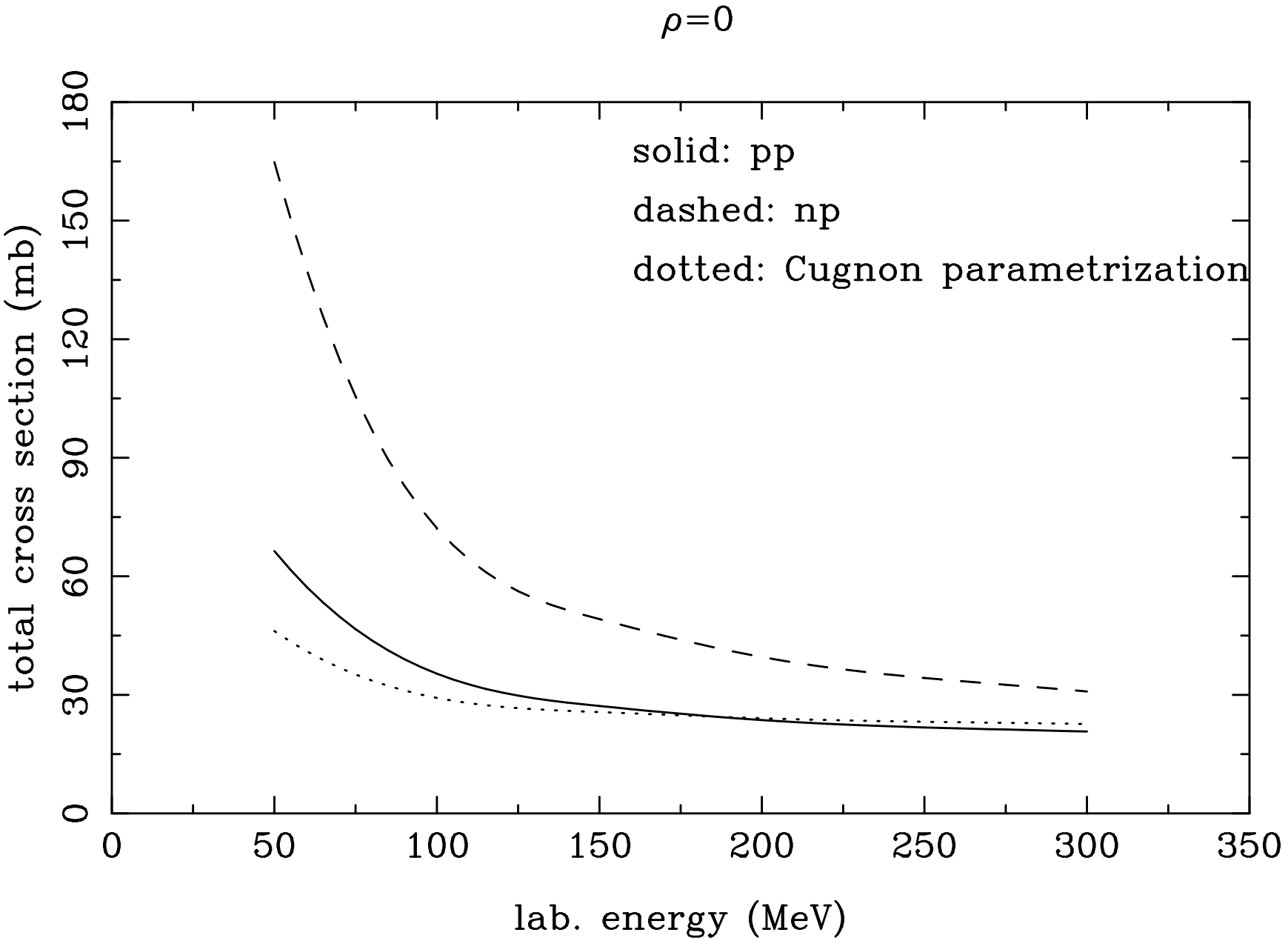
ρ=0
solid: pp
dashed: np
dotted: Cugnon parametrization
total cross section (mb)
0
30
60
90
120
150
180
0
50
100
150
200
250
300
350
lab. energy (MeV)

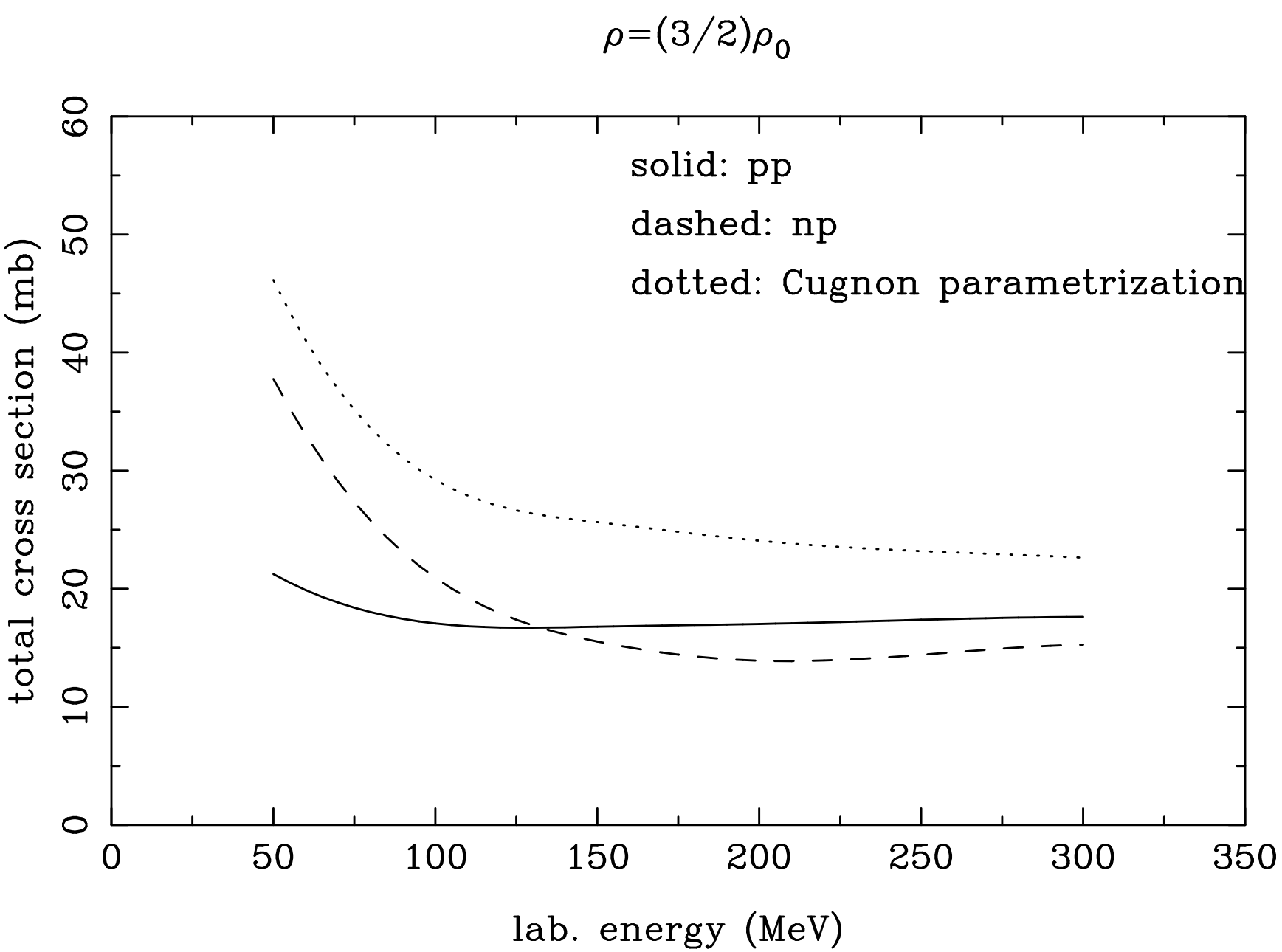
$\rho=(3/2)\rho_0$
solid: pp
dashed: np
dotted: Cugnon parametrization
total cross section (mb)
lab. energy (MeV)
0
10
20
30
40
50
60
0
50
100
150
200
250
300
350